Nuclear Engineering and Technology 50 (2018) 1173–1183

Contents lists available at ScienceDirect

Nuclear Engineering and Technology

journal homepage: www.elsevier.com/locate/net

Technical Note

Numerical prediction of a flashing flow of saturated water at high pressure

Jong Chull Jo [a, b, *], Jae Jun Jeong [b], Byong Jo Yun [b], Frederick J. Moody [c]

[a] Korea Institute of Nuclear Safety, Reactor System Evaluation Dept., 62 Gwahak-ro, Yusung-gu, Daejon, 34142, South Korea
[b] Pusan National University, School of Mechanical Engineering, 63 Busandaehak-ro, Geumjeong-gu, Busan, 46241, South Korea
[c] Consultant, 2125 N. Olive Ave. D-33, Turlock, CA, 95382, USA

ARTICLE INFO

Article history:
Received 20 February 2018
Received in revised form
27 May 2018
Accepted 3 June 2018
Available online 7 June 2018

ABSTRACT

Transient fluid velocity and pressure fields in a pressurized water reactor (PWR) steam generator (SG) secondary side during the blowdown period of a feedwater line break (FWLB) accident were numerically simulated employing the saturated water flashing model. This model is based on the assumption that compressed water in the SG is saturated at the beginning and decompresses into the two-phase region where saturated vapor forms, creating a mixture of steam bubbles in water by bulk boiling. The numerical calculations were performed for two cases of which the outflow boundary conditions are different from each other; one is specified as the direct blowdown discharge to the atmosphere and the other is specified as the blowdown discharge to an extended calculation domain with atmospheric pressure on its boundary. The present simulation results obtained using the two different outflow boundary conditions were discussed through a comparison with the predictions using a simple non-flashing model neglecting the effects of phase change. In addition, the applicability of each of the non-flashing water discharge and saturated water flashing models for the confirmatory assessments of new SG designs was examined.

1. Introduction

For the structural integrity evaluation of a PWR SG performed in the process of design or licensing review, it is required to know the transient hydraulic loading on the SG tubes and other internal structures during blowdown following any of the two design basis accidents (DBAs), such as a FWLB and a main steam line break (MSLB).

Even though many experimental and numerical studies were performed to simulate the transient thermal-hydraulic responses of a PWR SG to either FWLBs or MSLBs [1–10], only few studies addressing multi-dimensional numerical simulations of the thermal-hydraulic responses to a sudden FWLB are found in the literature. Recently, Jo et al. [11] performed a numerical simulation of the transient flow field inside the secondary side of a PWR SG [12] during blowdown following a FWLB. The non-flashing water flow through the broken feedwater pipe was assumed to estimate the transient blowdown loading conservatively.

Some investigators [13,14] reported that the highly pressurized subcooled liquid would discharge as a meta-stable liquid at a non-equilibrium state during blowdown of a liquid at a very high pressure to the atmosphere through very short pipes. In addition, it was reported in references [15–17] that the currently available two-phase critical flow models such as the Henry-Fauske model and the Moody model which have been widely employed in the reactor system design or safety analysis computer codes significantly underestimate the flowrates of subcooled water through pipes with $L/D \leq 3$ when compared to the experimental data. This is because subcooled water upstream the broken nozzle end may not be fully decompressed enough to reach the saturation pressure at the temperature of the subcooled water during the blowdown process. This implies that such two-phase critical flow situation would hardly occur during blowdown of a high pressure subcooled water through a short pipe.

The objective of this study is to re-examine the applicability of the two-phase critical flow model for the prediction of blowdown flow following a FWLB as indicated in the previous experimental

* Corresponding author. Korea Institute of Nuclear Safety, Reactor System Evaluation Dept., 62 Gwahak-ro, Yusung-gu, Daejon, 34142, South Korea.
E-mail addresses: jcjo@kins.re.kr, jongcjo@pusan.ac.kr (J.C. Jo), jjjeong@pusan.ac.kr (J.J. Jeong), bjyun@pusan.ac.kr (B.J. Yun), fred.j.moody@gmail.com (F.J. Moody).

https://doi.org/10.1016/j.net.2018.06.002

studies [15,16]. Thus a high pressure saturated water flashing flow through a broken feedwater pipe of a PWR SG [12] was numerically modelled. For this high pressure saturated water flashing flow situation, the transient flow field inside the SG secondary side was calculated employing a commercial CFD code [18]. Two different outlet boundary models of the saturated water flashing flow were applied to the calculations and the results predicted by both models were compared with each other. Finally, the present simulation results were discussed through a comparison with the predictions using a simple non-flashing model neglecting the effects of phase change to examine the applicability to the practical safety confirmation calculations.

2. Analysis

2.1. Analysis model

The PWR SG [12] considered in this paper is equipped with two economizer feedwater nozzles and one downcomer feedwater nozzle. During the normal SG full power operation, the economizer feedwater line supplies continuous feedwater flow to makeup 90 % of the SG's maximum steaming rate while the downcomer feedwater line accommodates 10 % of the total feedwater flow. It is assumed that a FWLB occurs during the SG full power operation or hot standby modes at the weld point of either of the two economizer feedwater nozzles, which is located nearest to the SG. If a feedwater line is broken suddenly at the welded location between a feedwater nozzle and its connected feedwater pipe, the feedwater flowing into the SG secondary side through the feedwater pipe will be interrupted and then the water in the SG secondary side will flow in the reverse direction to the broken feedwater nozzle end.

The purpose of this study is to develop a methodology and related techniques to numerically simulate the transient thermal hydraulic response to a FWLB and to investigate the general effects of the flashing blowdown flow on the SG secondary side flow condition. This paper does not address any comprehensive quantitative validation of the present analysis model but some qualitative investigation of its physical plausibleness by comparisons with other predictions.

In this respect, the physical SG model was simplified as a vertical once-through SG to which a feedwater pipe is attached to effectively simulate the saturated water flashing from the SG following the FWLB accident. The simplified FWLB model as shown in Fig. 1 was designed for the present numerical analysis to avoid extreme computational time and cost.

The analysis model considered in this paper is not a representative model but a sample one that maintains an actual value of the porosity inside a nuclear SG design to consider the flow resistances by the tubes and internal structures.

The SG vessel of the simplified model consists of 8.0 m and 4.0 m long stacked cylindrical spaces of 4.0 m diameter. Although the diameter of the upper steam space is larger than that of the lower part, this difference in diameter is disregarded in the present analysis because such difference would not affect the transient hydraulic response of the SG lower part to the FWLB significantly.

The existence of SG tube bundle was considered in the present analysis to simulate the transient decompression wave travelling through the tube-to tube gap space, which enabled calculations of the transient velocity or pressure distributions around the tubes. The SG tube bundle is modelled simply as 25 straight circular tubes of 0.6 m diameter of which the lower part is wetted by saturated water while the upper part is exposed to saturated steam. The tube bundle is located in the lower cylindrical space. The lower space of the SG secondary side has a porosity of 0.56 which is almost close to the value in an actual SG design. A horizontal pipe of 0.3 m diameter simulates the FW line with a break location 0.5 m from its attachment at the bottom of the model SG.

The reasons why the simplified tubes are included in the analysis model are to show how to predict the fluctuating (oscillating) velocities and pressures in the SG secondary side of the space between the tubes and the hydrodynamic loads on the tube surfaces. The works for evaluating the uncertainties introduced in our modeling approach and results as a consequence of the simplification are beyond the scope of this study. Some more realistic analysis models with the whole or any part of thousands U-bend tubes can be simulated by expending the computation cost and time much more.

2.2. Governing equations

The numerical model for calculating the transient three-dimensional turbulent flow in the PWR SG secondary side and flashing flow through a broken feedwater nozzle (or pipe) end following the FWLB was mathematically formulated. For the calculation of the two-phase flow during saturated water flashing from the SG at high pressure through the broken feedwater pipe, the inhomogeneous two-fluid model was used. Thus, the present problem was mathematically formulated with the governing equations consisting of two different sets of the mass, momentum and energy conservation equations for each of the two different inhomogeneous fluids (i.e. saturated water and steam). The turbulent viscosities were estimated by applying the $k-\omega$ based shear stress transport (SST) turbulence model [19]. The properties of the saturated water or steam were retrieved from the database in the CFD code.

For simplicity, the governing equations were expressed as a single set of the mass, momentum and energy conservation equations for any one of the two different phase fluids by using the low case Greek symbols α and β to denote either the saturated water and steam phases or the saturated steam and water phases interchangeably.

The governing equations for phase α fluid in a Cartesian coordinate system are given as follows:

2.2.1. Mass conservation equation for phase α

$$\frac{\partial}{\partial t}(f_\alpha \rho_\alpha) + \frac{\partial}{\partial x_j}(f_\alpha \rho_\alpha V_{\alpha,j}) = \Gamma_{\alpha\beta} - \Gamma_{\beta\alpha} \tag{1}$$

where $t, x_j (j = 1, 2, 3)$, f_α, ρ_α, and $V_{\alpha,j} (j = 1, 2, 3)$ represent time, three-dimensional components of the Cartesian coordinate system, volume fraction, density, and velocity field of phase α, respectively.

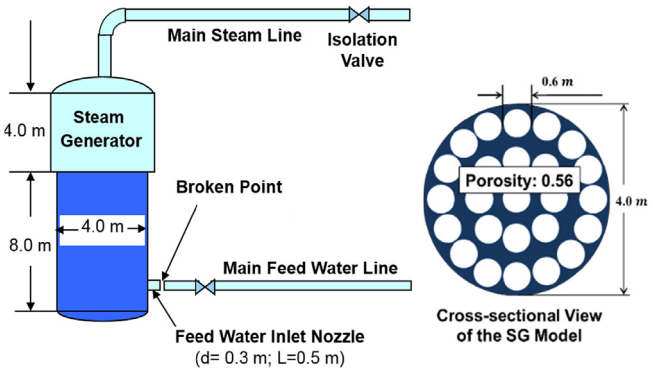

Fig. 1. Simplified FWLB analysis model [12].

In addition, $\Gamma_{\alpha\beta}$ and $\Gamma_{\beta\alpha}$ are the mass flow rates per unit volume from phase β to phase α and from phase α to phase β, respectively.

2.2.2. Volume conservation equation

$$f_\alpha + f_\beta = 1 \tag{2}$$

where f_β is the volume fraction of phase β.

Modeling the Reynolds stress term using the eddy viscosity hypothesis, the momentum conservation equation for the fluid can be expressed as follows:

2.2.3. Momentum conservation equation for phase α

$$\begin{aligned}&\frac{\partial}{\partial t}\left(f_\alpha \rho_\alpha V_{\alpha,i}\right) + \frac{\partial}{\partial x_j}\left(f_\alpha \rho_\alpha V_{\alpha,i} V_{\alpha,j}\right) + f_\alpha \frac{\partial p_\alpha}{\partial x_i} \\ &= \frac{\partial}{\partial x_j}\left(f_\alpha \mu_{eff,\alpha}\left(\frac{\partial V_{\alpha,i}}{\partial x_j} + \frac{\partial V_{\alpha,j}}{\partial x_i}\right) - \frac{2}{3}\rho_\alpha k_\alpha \delta_{ij}\right) + S_{M,\alpha} + M_\alpha\end{aligned} \tag{3}$$

where

$$\mu_{eff,\alpha} = \mu_{l\alpha} + \mu_{t\alpha} \tag{4}$$

where $\mu_{l\alpha}$, $\mu_{t\alpha}$, p_α, k_α, and $\delta$are laminar and turbulent viscosities, pressure, turbulence kinetic energy of phase α, and Kronecker delta function, respectively. The terms $S_{M,\alpha}$ and M_α in the right hand side of Eq. (3) respectively represent the momentum source due to buoyancy force acting on phase α and the sum of interfacial forces acting on phase α due to the presence of phase β, i.e., drag forces and momentum transfer associated with inter-phase mass transfer etc. $M_\alpha$is expressed as

$$M_\alpha = c_{\alpha\beta}^{(d)}\left(V_\beta - V_\alpha\right) + \left(\Gamma_{\alpha\beta} V_\beta - \Gamma_{\beta\alpha} V_\alpha\right) \tag{5}$$

The interphase drag coefficient $c_{\alpha\beta}^{(d)}$ for particle model is given as

$$C_{\alpha\beta}^{(d)} = \frac{C_{D_\alpha}}{8} a_{\alpha\beta} \rho_\alpha \left|V_\beta - V_\alpha\right| \tag{6}$$

where$a_{\alpha\beta}$is the interphase contact area given as

$$a_{\alpha\beta} = \frac{6 f_\beta}{d_\beta} \tag{7}$$

where phase $\beta$is assumed to be present as dispersed spherical particles with a mean diameter of $d_\beta$when phase α is assumed to be a continuous phase.

2.2.4. The drag coefficient$C_{D\alpha}$is given as

$$C_{D_\alpha} = \frac{D}{\frac{1}{2}\rho_\alpha \left(V_\alpha - V_\beta\right)^2 a} \tag{8}$$

where$\rho_\alpha$is the fluid density, the term $(V_\alpha - V_\beta)$ is the relative speed, $D$is the magnitude of the drag force and a is the projected area of the body in the direction of flow.

Because two phases share the same pressure field, the pressure constraint for both phases is given as

$$p = p_\alpha = p_\beta \tag{9}$$

Modeling the Reynolds flux term by using the eddy diffusivity hypothesis, the energy conservation equation for the fluid with a constant density can be expressed as follows:

2.2.5. Energy conservation equation for phase α

$$\begin{aligned}&\frac{\partial}{\partial t}\left(f_\alpha \rho_\alpha h_{tot,\alpha}\right) + \frac{\partial}{\partial x_j}\left(f_\alpha\left(\rho_\alpha V_{\alpha,j} h_{tot,\alpha} - A_{eff,\alpha}\frac{\partial h_{static,\alpha}}{\partial x_j}\right)\right) \\ &= f_\alpha \frac{\partial p_\alpha}{\partial t} + \left(\Gamma_{\alpha\beta} h_{tot,\beta s} - \Gamma_{\beta\alpha} h_{tot,\alpha s}\right) + Q_{\alpha\beta}\end{aligned} \tag{10}$$

where

$$h_{tot,} = h_{static,} + \frac{1}{2} V_{i,\alpha} V_{i,\alpha} \tag{11}$$

$$A_{eff,\alpha} = A_\alpha + \frac{\mu_{t,\alpha}}{Sc_{t,\alpha}} \tag{12}$$

$$A_\alpha = \frac{\lambda_\alpha}{c_{p,\alpha}} \tag{13}$$

$$Sc_{t,\ \alpha} = \frac{\mu_{t,\alpha}}{A_{t,\alpha}} \tag{14}$$

where $h_{static,\alpha}$, p_α, A_α, $A_{t,\alpha}$, $Sc_{t,\alpha}$, λ_α and $c_{p,\alpha}$ respectively represent static enthalpy, static pressure, diffusivity, turbulent diffusivity, Schmidt number ($= \mu_{t,\alpha}/A_{t,\alpha}$), thermal conductivity and specific heat capacity of the phase α fluid component. $Q_{\alpha\beta}$ in Eq. (10) indicates interphase heat transfer to phase α across the interface with phase β.

2.2.6. Turbulence model

To solve the above conservation equations, the turbulent viscosity $\mu_{t,\alpha}$ is calculated using the turbulence kinetic energy and its frequency $(k-\omega)$ based shear stress transport (SST) model [19].

It is well known that the $k-\omega$ based SST model developed by Menter, F. R [19]. simulates adverse pressure gradients and separating flow and also produces a wide range of turbulence levels in regions with large normal strain, including stagnation regions and regions with strong acceleration. Therefore the $k-\omega$ based SST model was used to estimate the turbulent viscosity $\mu_{t,\alpha}$ in this study.

It is known that this turbulence model, in combination with an optimal automatic wall treatment, provides highly accurate results for turbulent flow cases with a wide range of Reynolds number including sublayer flow [18].

This $k-\omega$ based SST model defines the turbulent viscosity μ_t having the following relationship with k and ω :

$$\mu_t = \frac{a' \rho k}{\max(a'\omega, SF_1)} \tag{15}$$

where

$$|S|^2 = S_{ij} S_{ij} \tag{16}$$

$$S_{ij} = \frac{1}{2}\left(\frac{\partial U_i}{\partial x_j} + \frac{\partial U_j}{\partial x_i}\right) \tag{17}$$

$$F_1 = \tanh\left((\arg 1)^2\right) \tag{18}$$

$$arg1 = \max\left(\frac{2\sqrt{k}}{\beta' \omega y}, \frac{500\nu}{\omega y^2}\right) \tag{19}$$

where ν and y represent the kinematic viscosity ($=\mu/\rho$) and the distance to the nearest wall boundary, respectively.

This SST model was derived by blending the $k-\omega$ turbulent model the $k-\varepsilon$ turbulent model which are well known to predicts the viscous wall boundary layer and its outer turbulent region of pipe flow field, respectively. In this blending process, the constant a' was fitted to 0.31 and the constant β' of 0.09 was derived. The $k-\omega$ based SST model including both constants has been used widely without any further validation.

Thus, the system of the governing equations is closed with two additional transport equations for k and ω that yield the turbulent viscosity μ_t.

2.2.7. Thermal phase change model

The positive mass flowrates per unit volume between both phases α and β expressed as $\Gamma_{\alpha\beta}$ and $\Gamma_{\beta\alpha}$, which are involved in the mass, momentum and energy conservation equations, are calculated using the following thermal (bulk) phase change model.

For the transfer processes across a phase interphase, the volumetric mass flowrate $\Gamma_{\alpha\beta}$ is expressed in terms of mass flux $\dot{m}_{\alpha\beta}$ and interphase area $a_{\alpha\beta}$ as

$$\Gamma_{\alpha\beta} = \dot{m}_{\alpha\beta} a_{\alpha\beta} \tag{20}$$

The mass flux from phase α into phase β, $\dot{m}_{\alpha\beta}$ is given as

$$\dot{m}_{\alpha\beta} = \frac{q_{\alpha s} + q_{\beta s}}{h_{\beta s} - h_{\alpha s}} \tag{21}$$

where $q_{\alpha s}$ and $q_{\beta s}$ are the sensible heat flux to phase α from the interface and that to phase β, respectively. $h_{\alpha s}$ and $h_{\beta s}$ represent interfacial values of enthalpy carried into and out of the phases due to phase change, respectively.

The governing equations for phase β are given in the same manner as above by interchanging the subscript symbols α and β. The whole set of the conservation equations for the two different phases α and β are solved by closing with a relation among pressure, molecular volume and temperature of the fluids.

In addition, the fluid properties for thermodynamics are needed to solve the energy equation when the working fluid region is compressible. In the present simulation, the properties of the working fluid are retrieved directly from the database in a tabular form built in the CFX code [18].

2.3. Boundary and initial conditions

The upper and lower spaces of the SG were assumed to be initially occupied with saturated steam and water at a constant pressure of 7.5*MPa* . The FWLB was assumed to occur at the weld point between the SG feedwater inlet nozzle and the feedwater supplying pipe in a very short time. This was modeled by defining a linear pressure decrease from the initial state to the atmospheric pressure in 1.0 *ms* at the broken end of the feedwater inlet nozzle. The main steam isolation valves of the SG were assumed to be closed instantly following the FWLB. The no-slip and adiabatic boundary conditions were specified to the solid wall inner-surfaces of which the outer-surfaces are insulated to prevent heat loss. The volumes of saturated steam and water were set to initially occupy the upper and lower spaces, respectively. The initial water level $z_{w_0} = 8.0\ m$ and the initial velocity $V_0 = 0.0\ m/s$ were given. Such no-flow condition was assumed to be likely at the switchover moment when all the flows in the calculation domain including the SG secondary side and the attached feedwater inlet nozzle simultaneously become to reverse from feeding into the SG to discharging from the SG due to a sudden break of the feed pipe.

One of the two different outlet boundary models of the flashing flow through the broken nozzle (Model 1) was modeled by limiting the numerical simulation domain to the broken nozzle end cross-section at which the atmospheric pressure was specified after the pipe break, as shown in Fig. 2(a).

The other (Model 2) was modeled, as shown in Fig. 2(b), by extending the simulation domain to a cylindrical-shaped ambient space surrounding the broken nozzle end. The cylindrical ambient space was initially maintained at the atmospheric pressure. The boundaries of the cylindrical simulation domain are comprised of the solid concentric bottom surface boundary surrounding the cross-sectional flow area of the broken nozzle end and the permeable side wall surface and circular top surface boundaries at which the constant atmospheric pressure of 0.1 *MPa* is maintained throughout the blowdown period.

2.4. Numerical analysis

A mesh (grid structure and size) sensitivity study to determine an optimum discretization of the solution domain needs to be performed for assuring accuracy of the numerical calculation results. The numerical computation for the present problem required very long time with a high performance computing system as in the previous numerical calculations of unsteady phase change flows in complex systems [7,10]. For information, it took over 20 CPU days to perform the parallel computation of the transient flashing flow for the simulation time period of 1.0 *s* using 48 cores. As such, the calculations of the present model are costly.

As mentioned previously, the purpose of this study is to develop a methodology and related techniques to numerically simulate the SG secondary flow field following a FWLB and the aim for publishing this paper is to share the authors' idea and experience in numerical modelling of the subcooled liquid non-flashing, saturated liquid flashing and subcooled liquid non-flashing flows in an efficient way. In this regard, this paper did not address any comprehensive quantitative validation of the present analysis model but some qualitative investigation of its physical plausibleness by comparisons with other predictions.

For these reasons, the calculation domain for the present work was discretized as fine as reasonably practicable based on the authors' experience in the previous works although the mesh sensitivity study was not performed.

As shown in Fig. 2, the whole calculation domain of the two outlet boundary models including the SG, the inlet nozzle of the feedwater pipe, and the outer ambient space of the broken nozzle end (only for Model 2) was discretized into fine meshes of 1,440 K and 1,800 K sweep or tetra elements, respectively. The tetra elements were used for discretization of the junction area between the SG cylinder and the feedwater inlet nozzle.

Based on the result of the sensitivity study of acceptable time step sizing for the present transient numerical calculations, time steps ranging from 0.001 *ms* to 0.01 *ms* were applied. The Courant

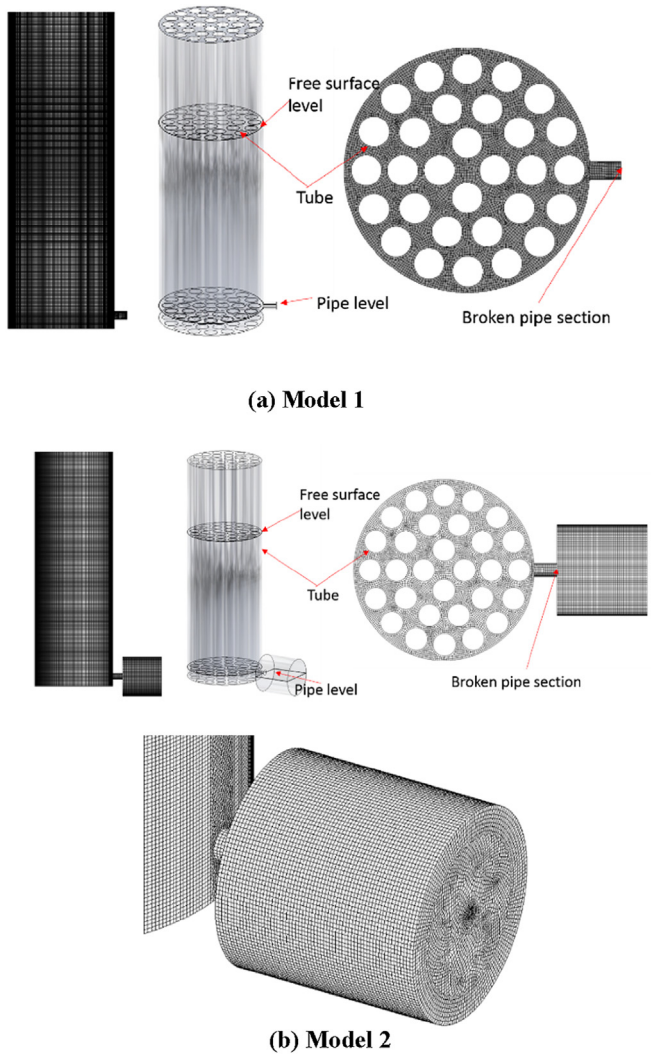

Fig. 2. Saturated water flashing flow analysis models.

numbers (defined as the product of the fluid flow or pressure wave velocity and the time step size divided by the mesh size in the one-dimensional flow case) in the broken feedwater nozzle flow domain were estimated to have small values of less than 1.0, based on the maximum fluid velocity of about 80 m/s and the upper limiting pressure wave velocity of about 1,500 m/s, the maximum time step size of about 0.01 ms, and the minimum mesh size of 0.02 m in the main flow direction along the feedwater nozzle.

The present CFD analysis procedure is as follows. A linear set of discrete conservation equations is obtained by applying the finite element method-based finite volume method and is assembled into the solution matrix. The convection terms are dealt with applying the 2nd order bounded high resolution scheme. The diffusion terms are treated by applying central differential scheme. The transient terms are approximated by the 1st order backward Euler scheme. Potential pressure-velocity decoupling in the discretized momentum equation is avoided by applying the momentum interpolation scheme, which was proposed by Rhie and Chow [20] and later modified by Majumdar [21]. The solution variation within a control volume is calculated with finite element shape functions which are linear in terms of parametric coordinates. The derivatives for all the diffusion terms are estimated by the use of shape functions, following the standard finite element approach. The pressure gradient term is also estimated using the shape functions. The coupled hydrodynamic equations for three components of velocity vector in Cartesian coordinates and pressure as a single system are solved by employing an algebraic multigrid method. The unsteady terms are treated fully implicitly at any specified time step. For the calculation of shell side and feedwater pipe inside multiphase flow accompanying the phase change, the inhomogeneous two-fluid model is used.

The analysis model at the steady-state condition was calculated for 0.01 s to obtain the initial pressure distribution in the model using the time marching technique. An iterative computation for each time step was set to terminate when the maximum of the absolute sum of dimensionless residuals of governing equations becomes smaller than 0.0001.

The transient velocity and pressure of fluid were monitored at 6 different locations “Point 1~Point 5” and the exit section as shown in Fig. 3. In the exit section, area averaged values of velocity and pressure were monitored.

3. Results and discussion

3.1. Typical results of the numerical simulations

The numerical method applied to the present calculations was validated in the previous work [8], where the numerical analysis model was applied to simulate the same blowdown situation as in an experimental study [9] which was conducted for a simplified SG blowdown model, and the numerical results were shown to be in a reasonably good agreement with the measurements.

Figs. 4–8 show some typical calculation results of the transient fluid velocity, pressure and blowdown flowrate responses to the FWLB for the two different outlet boundary models. Figs. 4 and 5 respectively display the transient steam velocity and pressure contours around the broken nozzle end at the elapsed times of 0.001 s and 0.1 s after the FWLB for the two boundary models. In particular, Model 2 enables to simulate the rapidly expanding velocity disturbances generated from the broken nozzle end just following the pipe break. Fig. 4 shows that the radially expanding steam speed in the front part of the velocity disturbance wave is supersonic while the expanding steam near the broken nozzle end maintains sonic speed.

The transient steam velocity contours of Model 2 at 0.1 s shows some steep changes and distorted shapes nearby the atmospheric pressure boundaries. This is because the calculation domain for simulating the infinite ambient space with constant atmospheric pressure boundaries was not enough to accommodate the expanding steam velocity waves for relatively long time periods of blowdown so that the expanding velocity or pressure disturbances were distorted. Therefore, the present calculation domain of the ambient would be valid only for the early time period of blowdown until the frontal surface of the expanding steam velocity or pressure disturbances downstream the broken nozzle end reaches any part of the calculation domain boundaries at which a constant atmospheric pressure condition is specified. Consequently, to simulate the discharged steam flow field in the ambient for a specified time period of blowdown, the calculation domain should be extended much further in proportion to the time period.

However, it is considered that the effects of the size of the present calculation domain outside the broken nozzle end on the transient responses of water velocity or pressure disturbances inside the SG secondary side would not be significant because the discharging steam pressure disturbances seems to be attenuated rapidly in the ambient space. Fig. 5(b) displays transient pressure contours in the SG secondary side region at 0.2 s. As shown in the figure, the pressure distributions nearby the centerline between the feedwater pipe nozzle inlet and the point on the opposite SG

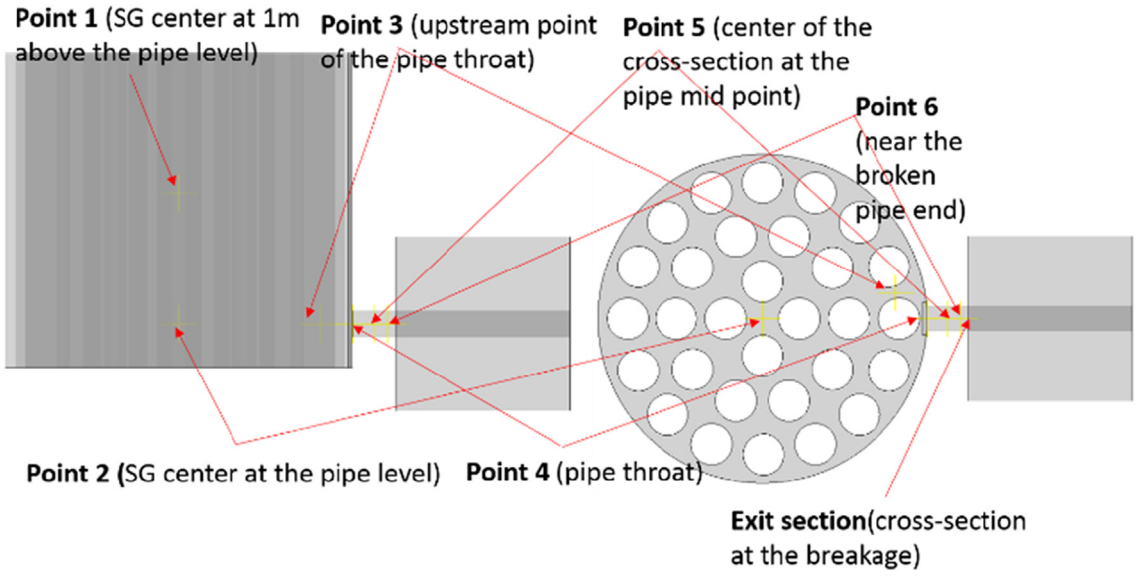

Fig. 3. Monitoring points.

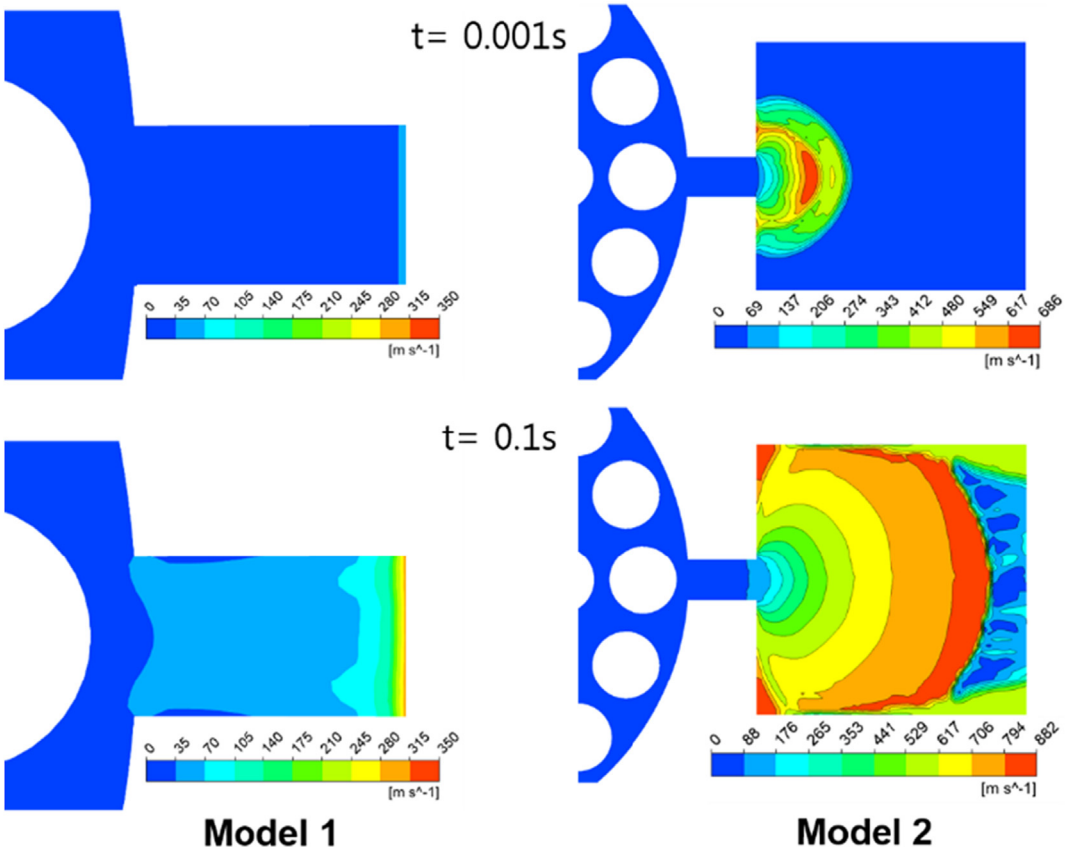

Fig. 4. Transient steam velocity contours at 0.001 *s* and 0.1 *s*.

inner wall were predicted by both models closely while those in the peripheral regions where are the left and right hand-sides of the centerline are somewhat different.

Generally, Model 2 predicted more severe pressure gradients across the tubes than Model 1. This implies that Model 2 would yield more conservative prediction of transient hydraulic loads inside the SG secondary side than Model 1. Based on the above discussion, it is seen that Model 2 would predict the thermal-hydraulic responses in the flow field downstream the broken nozzle end following the FWLB more realistically than Model 1.

Fig. 6 displays the transient water velocity responses of the six different monitoring points over the elapsed time of 0.2 *s* after the

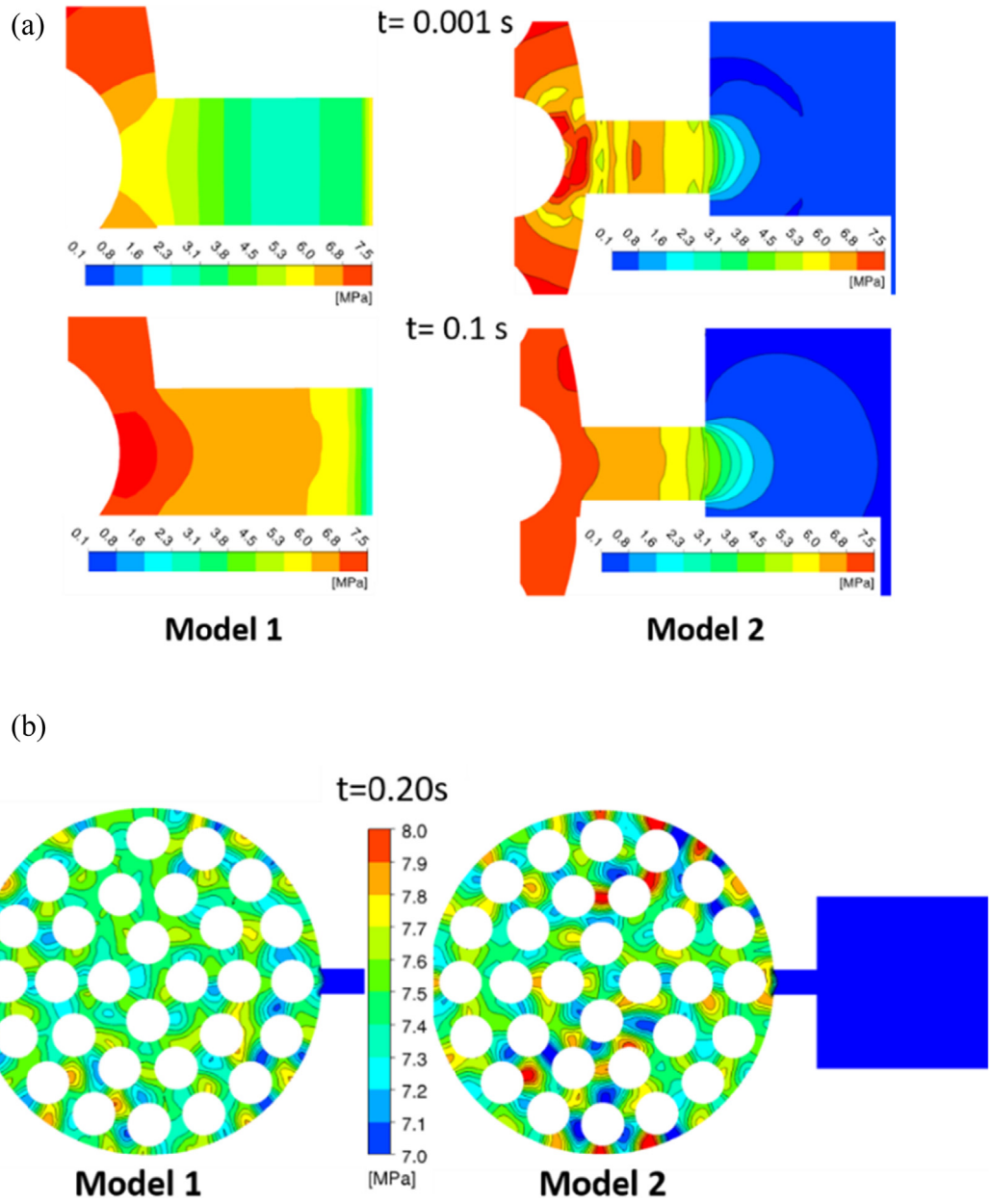

Fig. 5. (a). Transient pressure contours in the broken feed pipe region at 0.001 *s* and 0.1 *s*, (b). Transient pressure contours in the SG secondary side region at 0.2 *s*.

FWLB for the two outlet boundary models. Although both Model 1 and Model 2 seem to yield little differences in the calculation results during the specified blowdown time period, the calculations at other local points in the peripheral areas apart from the SG centerline extending the feedwater pipe might show significant differences (see Fig. 5(b)).

Fig. 7 shows the transient pressure responses of the four different monitoring points during the early blowdown over the elapsed time of 0.25 *s* after the FWLB for the two outlet boundary models. The solid line with the symbol "diamond" and the dotted line with the symbol "inclined triangle" are identified as the uppermost plot and the next uppermost one, respectively. As seen from Fig. 7, Model 1 yields more fluctuating transient pressure disturbances during the early time period of blowdown over the elapsed time of 0.1 *s* because it assumes the linear ramp change in pressure at the broken nozzle end at the beginning of blowdown in Model 1.

Fig. 8 displays the transient blowdown flowrate responses to the FWLB in the two outlet boundary models. As shown in Fig. 8, Model 1 predicts the mass flowrate about 1.3 times higher than Model 2 at the very beginning stage of blowdown while the transient responses of mass flowrate predicted by both models show little differences from the elapsed time of 0.03 *s* after the pipe break.

In general, the simulation results for both models are somewhat different from each other at the very beginning of blowdown and in the flow field near the broken nozzle end. It is seen that Model 2 extending the simulation domain to an atmospheric space surrounding the broken nozzle end can yield more comprehensive simulation results of the present blowdown problem than the simpler Model 1. This is because the use of the outlet boundary condition Model 2 results in a detailed simulation of the flow field near the broken nozzle end including particularly the ambient space downstream the blowdown exit.

The oscillations with the frequency of about 30 cycles shown in

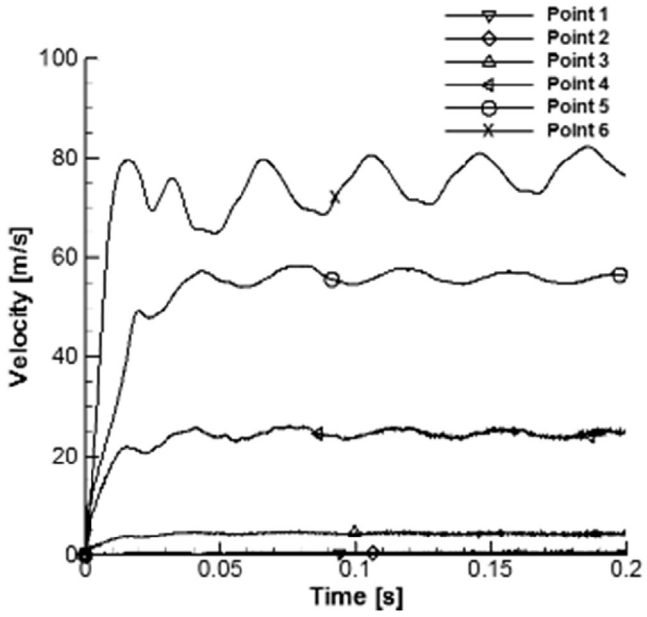

Model 1

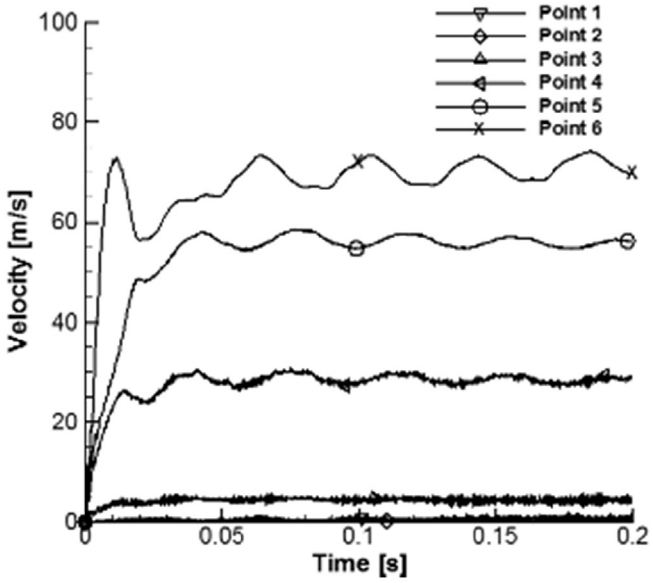

Model 2

Fig. 6. Transient water velocity responses at the 6 monitoring points.

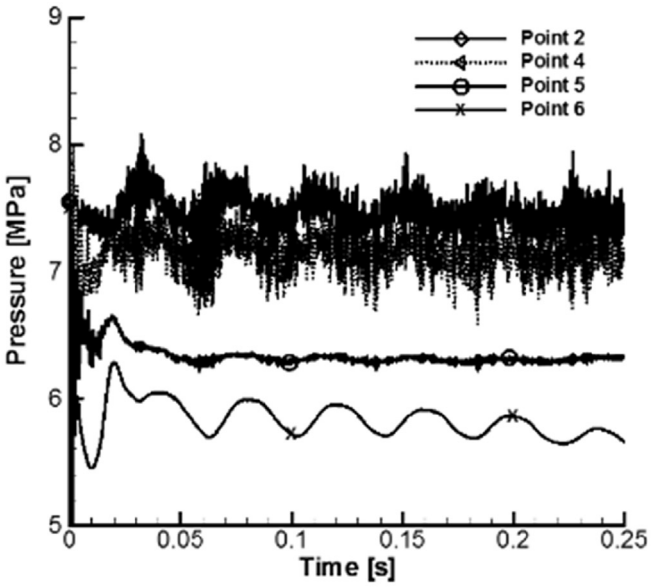

Model 1

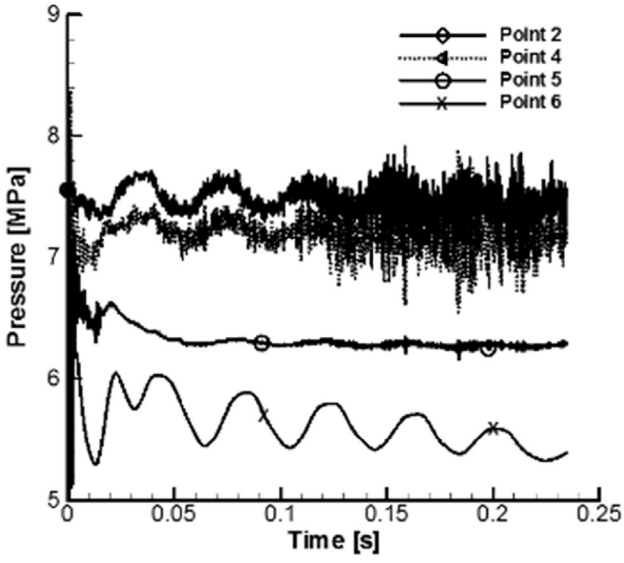

Model 2

Fig. 7. Transient pressure responses at the 4 monitoring points.

Figs. 6–8 are the decompression wave of water hammer which travels between the broken pipe end and the SG inner wall, which was discussed in detail in the previous works [7,11]. The noise-like small amplitude oscillations on the trajectory of the oscillations of decompression wave inside the SG are resulted from multiple reflections of the decompression wave by the top, bottom and cylindrical wall of the SG inner space.

This numerical simulation is an approach for obtaining the actual flowrate without using the concept of discharge coefficient C_d for accounting for the non-ideal effects, which is defined as the ratio of the actual flowrate Q_{actual} to the ideal (inviscid) flowrate Q_{ideal} based on the Bernoulli relation. The work for predicting the discharge coefficients is out of the scope of the present study because any correlation for modelling the critical flow at the broken pipe end is not employed in the present CFD calculations. Nevertheless, the flowrate $Q_{cal.}$ calculated from the present numerical simulation can be used to estimate the discharge coefficient C_d under assumptions that the calculated flowrate $Q_{cal.}$ would be close to the actual flowrate Q_{actual} (i.e. $Q_{cal.} \approx Q_{actual}$) and the ideal flowrate Q_{ideal} could be defined along the streamline outside the broken pipe end.

3.2. Comparisons of the saturated water flashing flow model to the subcooled water non-flashing flow model

At present, it is hard to find any available experimental data which are suitable for the use of comparison with the present

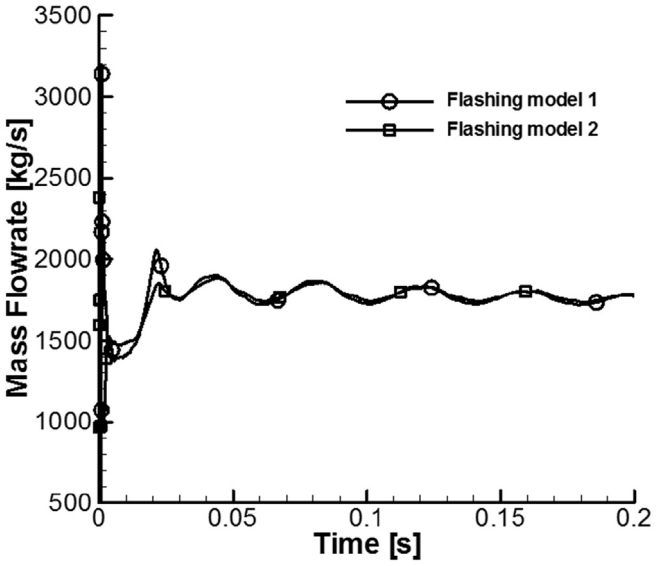

Fig. 8. Transient blowdown flowrates.

numerical results. Therefore, to investigate the applicability of the saturated water flashing flow model for the prediction of highly pressurized water discharging flow, the present numerical calculation results in terms of the blowdown flowrates from the broken feedwater inlet nozzle end and the water flow velocities in the SG secondary were compared with those predicted for the subcooled water non-flashing (discharging) flow model by CFD and/or simple methods.

3.2.1. Blowdown flowrates

At first, the calculated transient blowdown flowrates were compared to the steady-state subcooled water discharging flowrate estimated by a simple method and the transient blowdown flowrates by CFD method as shown in Fig. 8. The meta-stable non-flashing discharge model does not permit vapor bubbles to form an equilibrium saturated water/steam mixture during decompression between the SG and discharge plane. Bubble formation in the subcooled water is delayed, and the discharging fluid is in a non-equilibrium state close to that of pure water. The blowdown mass flux for subcooled water was formulated by Zaloudek for flow between the SG source pressure P_o and the saturation pressure $P_{sat}(T_o)$ [22,23], for which the discharge mass flux G_c is given by

$$G_c = \sqrt{2\rho_o(P_0 - P_{sat}(T_o))} \tag{22}$$

where ρ_o denotes the density of subcooled water.

For the subcooled water temperature T_o of 260 °C, the water density ρ_o is 789 kg/m^3 and the saturation pressureP_{sat} is 4.69 *MPa*. Thus,

$$G_c = \sqrt{2\text{x}789\text{x}(7.5 - 4.69)\text{x}10^6} = 66,590\left[kg\Big/m^2 \cdot s\right] \tag{23}$$

The corresponding steady-state mass blowdown rate is

$$\dot{m} = G_c a = 66,590 \text{ x } 0.0707 = 4,708\ [kg/s] \tag{24}$$

where a denotes the discharging flow area of the broken nozzle end.

For the subcooled water non-flashing flow model, the transient blowdown flowrates simulated by CFD [11] were much greater than the steady-state discharging flowrate of 4,708 kg/s estimated by the above simple method during the early stage of blowdown process as shown in Fig. 9 and were seen to approach gradually to the steady-state flowrate.

As such the subcooled water non-flashing flow model estimates the discharging flowrate greater compared to Zaloudek model because the no phase change is considered in the former model. Meanwhile, the present saturated water flashing flow model implies that the highly pressurized subcooled water discharging from the SG decompresses to the saturation pressure as it flows through the broken feedwater nozzle with forming steam bubbles in an equilibrium, homogeneous bubbly mixture, which reaches a critical flow value at the broken nozzle end. As shown in Fig. 9, the saturated water flashing flow model considerably underestimates the blowdown flowrates than the subcooled water non-flashing flow model because the blowdown flow is obstructed due to the rapid vaporization of the saturated water into steam and subsequent expansion of the steam as the decompression wave travels between the broken nozzle end and the SG following the FWLB. The corresponding discharge velocity predicted by Zaloudek model is obtained as

$$V = \frac{G_c}{\rho} = \frac{66,590}{789} = 84.4[m/s] \tag{25}$$

which is above the average velocity of 75 m/s of the point 6 trace marked with x axis in the feedwater discharge pipe for Model 1, shown in Fig. 6.

3.2.2. Flow velocities

The CFD calculations of the flow velocities inside the SG secondary side were compared to the rough estimations by a simple approach assuming a sink flow into the feedwater nozzle as follows. The discharge flowrate from the feedwater nozzle of a cylindrical pipe would draw fluid from all directions inside the SG if the inside volume was unobstructed.

However, the feedwater nozzle attachment (discharge outlet) is near SG vessel bottom surface which functions as an obstruction in the radial flow field upstream the outlet. To take into account such

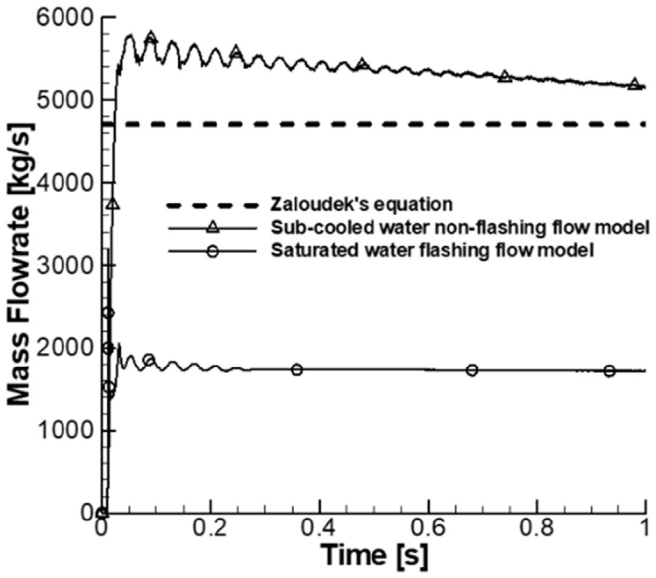

Fig. 9. Comparison between the blowdown flowrates predicted using the subcooled water non-flashing flow model and the saturated water flashing flow Model 1.

obstruction effect on the discharge flow field, a symmetric image feedwater sink below the SG vessel bottom was introduced to produce a flow boundary of zero vertical velocity across the SG bottom, as shown in Fig. 10. This symmetric image feedwater sink does not affect the estimated flowrates but only takes into account the effect of the solid bottom surface boundary condition on the flow field near the feedwater nozzle pipe attachment area, specifying that the water velocity component normal to the bottom surface is always zero.

Water discharge from the feedwater nozzle in this evaluation is treated as a sink flow with a volumetric flow rate Q given as

$$Q = aV \tag{26}$$

where a is the feedwater flow area and V is the fluid velocity.

For the non-flashing discharge of Model 1 above, the discharge velocity V of Eq. (25) gives the volume discharge rate as

$$Q = 0.0707 \times 84.4 = 5.97\left[m^3/s\right] \tag{27}$$

The volume flow rate Q into a point sink would flow through the hemisphere of an imaginary boundary inside the SG at the feedwater nozzle pipe attachment, whose area a_{hs} would be half of a sphere having a radius r which is equal to the feedwater nozzle.

$$a_{hs} = 2\pi r^2 = 2\pi \times 0.15^2 = 0.1414\left[m^2\right] \tag{28}$$

with a corresponding velocity across its surface of area a_{hs} (which is twice the feedwater nozzle area) of

$$V = 84.4/2 = 42.2[m/s] \tag{29}$$

The monitoring point 2 in the SG as shown in Fig. 3 is located at a distance about $r_2 = 2\ m$ away from the feedwater nozzle pipe attachment at about the same elevation. Its corresponding imaginary hemispherical area a_{hs2} at the monitoring point 2 (center at the same location as the feedwater hemisphere), in the absence of internal structures, would be

$$a_{hs2} = 2\pi r_2^2 = 2\pi \times 2^2 = 25.13\left[m^2\right] \tag{30}$$

Since the water actually flows across the upper half part (above the SG bottom surface) of the hemispherical area a_{hs2}, the local velocity V_2 at the monitoring point 2 which is unobstructed by SG tubes is related to the feedwater hemisphere velocity V according to mass conservation between both concentric hemispherical surfaces as

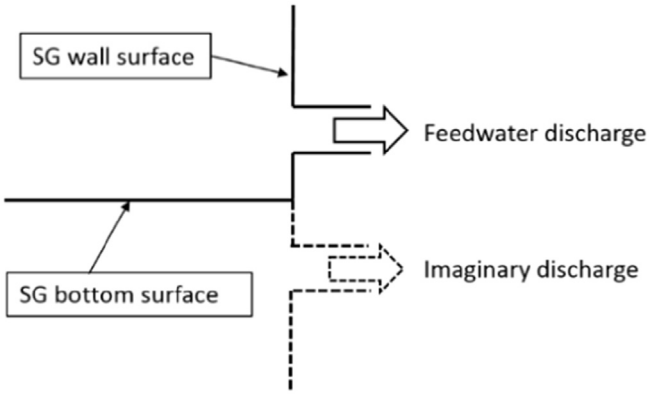

Fig. 10. Concept of a symmetric image feedwater sink.

$$V_2 = \frac{a_{hs}}{a_{hs2}/2} V = 2\left(\frac{r}{r_2}\right)^2 V \tag{31}$$

With the tube obstruction, the flow area at the point 2 will be decreased to a fraction equal to the porosity which is defined as a ratio of the unobstructed area to the total area, given as $\beta = 0.56$. It follows that the approximate water velocity between tubes at distance r_2 from the feedwater line attachment is estimated by

$$V_2 = \frac{2}{\beta}\left(\frac{r}{r_2}\right)^2 V \tag{32}$$

or for $r = 0.15\ m$, $r_2 = 2\ m$, $V = 42.2\ m/s$ and $\beta = 0.56$,

$$V_2 = \frac{2}{0.56}\left(\frac{0.15}{2.0}\right)^2 \times 42.2 = 0.84\ [m/s] \tag{33}$$

This estimated value 0.84 m/s of Eq. (33) is approximately close to the velocity at the point 2 predicted using the subcooled water non-flashing flow model [11] while it shows some difference from the prediction using the saturated water flashing flow model (see Fig. 11), as can be expected from Fig. 8.

Internal velocities from the non-equilibrium discharge model are higher, and will give larger, more conservative loads on SG internals.

4. Conclusions

This paper presented a comparison of the SG internal flow fields for a non-equilibrium subcooled water non-flashing discharge model and also for a saturated water flashing flow model following a FWLB. Transient SG internal flow fields and blowdown flow rates of a saturated water flashing flow model during a FWLB were predicted using two different outlet boundary models of the discharge region: one (Model 1) does not include any part of the ambient space outside the broken nozzle end and the other (Model 2) includes a finite ambient space of cylindrical shape just downstream the broken nozzle end.

It was shown that both models predicted the pressure

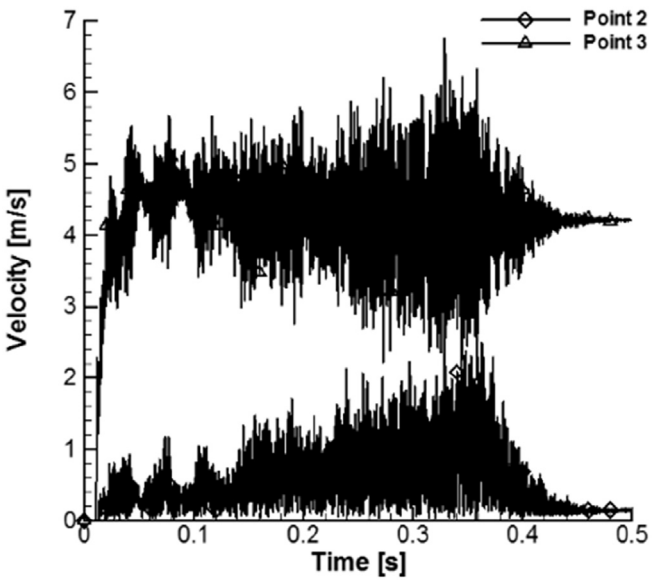

Fig. 11. Enlargement of the transient velocity responses at the monitoring points 2 and 3, predicted using the saturated water flashing flow model.

distributions at the monitoring points nearby or on the horizontal centerline between the feedwater pipe nozzle inlet and the opposite SG inner wall closely while the two predictions at other local points in peripheral regions inside the SG secondary side were somewhat different. In addition, it was found that Model 2 predicted the thermal-hydraulic responses in the flow field downstream the broken nozzle end following the FWLB more realistically compared to Model 1. To precisely simulate the discharged steam flow field in the ambient outside the broken nozzle end for a specified time period of blowdown using Model 2, the calculation domain for the ambient space should be extended appropriately considering the time period of the blowdown transient.

Meanwhile, the saturated water flashing flow model with either of the two outlet boundary models seem to considerably underestimate the discharging flowrates comparing to the subcooled water non-flashing flow model because the rapid vaporization of the saturated water and expansion of the vaporized steam obstruct the discharging mass flow. Thus, these saturated water flashing models are expected to provide non-conservative predictions of transient hydraulic loads acting on the SG tubes and their support structures in terms of transient velocity and pressure disturbances.

Based on the present CFD simulation results of the saturated liquid flashing-flow, the transient flowrate in the early stage of blowdown following a FWLB oscillates violently due to the decompression wave (resulting in the water hammer load) travelling between the blowdown exit and the SG inner wall and comes to stabilize gradually approaching the critical flowrate. The problem is that the existing critical flow models would not be appropriate to predict such transient thermal hydraulic response of the flashing flow because those correlations are based on the quasi-steady flow.

Therefore, for prediction of the transient hydraulic responses in the SG secondary side to the FWLB more realistically, an appropriate CFD calculation model for practical subcooled water flashing flows needs to be developed. At present, for conservative estimation of the SG structural integrity evaluation it is recommended to use the non-flashing model until any validated flashing flow calculation model becomes available.

Appendix A. Supplementary data

Supplementary data related to this article can be found at https://doi.org/10.1016/j.net.2018.06.002.

References

[1] S. Gallardo, A. Querol, G. Verdú, Simulation of a main steam line break with steam generator tube rupture using trace, in: Proceedings of the PHYSOR, American Nuclear Society, Knoxville, TN, USA, 2012, pp. 2131–2144.
[2] L. Wolf, Experimental results of coupled fluid-structure interactions during blowdown of the HDR-vessel and comparisons with pre- and post-test predictions, Nucl. Eng. Des. 70 (1982) 269–308.
[3] P. Saha, A. Ghosh, T.K. Das, S. Ray, Numerical simulation of pressure wave time history inside a steam generator in the event of main steam line break and feedwater line break transients, in: Proceedings of the Transient Phenomena in Nuclear Reactor Systems, ASME HTD-vol. 245/NE, vol. 11, 1993, pp. 131–140.
[4] H. Tinoco, Three-dimensional modeling of a steam-line break in a boiling water reactor, Nucl. Sci. Eng. 140 (2002) 152–164.
[5] K.H. Kang, H.S. Park, S. Cho, N.H. Choi, S.W. Bae, S.W. Lee, Y.S. Kim, K.Y. Choi, W.P. Baek, M.Y. Kim, Experimental study on the blowdown load during the steam generator feedwater line break accident in the evolutionary pressurized water reactor, Ann. Nucl. Ener 38 (2011) 953–963.
[6] O. Hamouda, D.S. Weaver, J. Riznic, Loading of Steam Generator Tubes during Main Steam Line Breaks, CNSC Contract No. 87055-11-0417– R430.3, RSP-0305, Canadian Nuclear Safety Commission, 2015.
[7] J.C. Jo, F.J. Moody, Transient thermal-hydraulic responses of the nuclear steam generator secondary side to a main steam line break, ASME JPVT 137 (2015), 041301-1-7.
[8] J.C. Jo, B.K. Min, J.J. Jeong, Evaluation of a numerical analysis model for the transient response of nuclear steam generator secondary side to a sudden steam line break, ASME JPVT 139 (2017), 041301-1-7.
[9] O. Hamouda, D.S. Weaver, J. Riznic, An experimental model study of steam generator tube loading during a sudden depressurization, ASME JPVT 138 (2016), 041302-1-11.
[10] J.C. Jo, F.J. Moody, Effects of a venturi type flow restrictor on the thermal-hydraulic response of the secondary side of a pressurized water reactor steam generator to a main steam line break, ASME JPVT 138 (2016), 041304-1-12.
[11] J.C. Jo, J.J. Jeong, F.J. Moody, Transient hydraulic response of a pressurized water reactor steam generator to a feedwater line break using the nonflashing liquid flow model, ASME JPVT 139 (2017), 031302-1-8.
[12] KHNP, APR+ Standard Safety Analysis Report, KHNP, Seoul, 2011.
[13] J. Weisman, A. Tentner, Models for estimation of critical flow in two-phase systems, Prog. Nucl. Ener 2 (1978) 183–197.
[14] J.R. Simones-Moreira, M.M. Vieira, E. Angelo, Highly expanded flashing liquid jets, J. Thermophysics Heat Transfer 16 (2002) 415–424.
[15] R.E. Henry, H.K. Fauske, The two-phase critical flow of one-component mixtures in nozzles, orifices, and short tubes, ASME J. Heat Transfer 93 (1971) 179–187.
[16] K.H. Ardron, R.A. Furness, A study of the critical flow models used in reactor blowdown analysis, Nucl. Eng. Des. 39 (1976) 257–266.
[17] D. Bestion, F. D'Auria, P. Lien, H. Nakamura, A State-of-the-art Report on Scaling in System Thermal Hydraulics Applications to Nuclear Reactor Safety and Design, OECD Nuclear Energy Agency, Paris, France, 2017. NEA/CSNI/R(2016)14.
[18] ANSYS CFX User's Guide-14, ANSYS Inc., NY, 2012.
[19] F.R. Menter, Two equation eddy-viscosity turbulence models for engineering applications, AIAA J. 32 (1994) 1598–1604.
[20] C.M. Rhie, W.L. Chow, Numerical study of the turbulent flow past an airfoil with trailing edge separation, AIAA J. 21 (1983) 1525–1532.
[21] S. Majumdar, Role of under-relaxation in momentum interpolation for calculation of flow with non-staggered grids, Num. Heat Transfer 13 (1988) 125–132.
[22] F.R. Zaloudek, The Critical Flow of Hot Water through Short Tubes, 1963. HW-77594, General Electric, WA, USA.
[23] L.S. Tong, J. Weisman, Thermal Analysis of Pressurized Water Reactors, ANS, La Grange Park, Il., USA, 1979.